Nanomed. J. 5(1): 36-45, Winter 2018

RESEARCH PAPER

Spectroscopic investigation on the interaction of DNA with superparamagnetic iron oxide nanoparticles doped with chromene via dopamine as cross linker

Maryam Mehdipour [1], Gholamreza Dehghan [1]*, Mohammad Ali Hosseinpour Feizi [1], Roghayeh Tarasi [2], Mehdi Khoobi [3,4], Siavoush Dastmalchi [5,6]

[1]Department of biology, Faculty of Natural Science, University of Tabriz, Tabriz, Iran

[2]Department of Chemistry, University of Zanjan, Zanjan, Iran

[3]Department of Pharmaceutical Biomaterials and Medical Biomaterials Research Center, Faculty of Pharmacy, Tehran University of Medical Science, Tehran, Iran

[4]Department of Medicinal Chemistry, Faculty of Pharmacy and Pharmaceutical Science Research Center, Tehran University of Medical Science, Tehran, Iran

[5]Biotechnology Research Center, Tabriz University of Medical Sciences, Tabriz, Iran

[6]Department of Medicinal Chemistry, School of Pharmacy, Tabriz University of Medical Sciences, Tabriz, Iran

ABSTRACT

Objective(s): The interaction of DNA with iron oxide nanoparticles (SPIONs) was studied to find out the interaction mechanism and design new drug delivery systems.

Materials and Methods: The interaction of calf thymus DNA (ctDNA) with SPIONs doped with 2H-chromene via dopamine as cross linker (SPIONs@DA-Chr) was studied using the UV absorption spectroscopy, viscosity measurement, circular dichroism, fluorescence and FT-IR spectroscopic techniques.

Results: UV absorption study showed hyperchromic effect in the spectra of DNA. Few changes were observed in the viscosity of ctDNA in the presence of different concentration of SPIONs@DA-Chr. The result of circular dichroism (CD) suggested that SPIONs@DA-Chr can change the secondary structure of DNA. Further, fluorescence quenching reaction of ctDNA with SPIONs@DA-Chr and competitive fluorescence spectroscopy studied by using methylene blue, have shown that the SPIONs@DA-Chr can bind to ctDNA through non-intercalative mode. FT-IR spectroscopy confirmed the binding of SPIONs@DA-Chr and ctDNA.

Conclusion: These results suggested that SPIONs@DA-Chr binds to DNA via groove binding mode.

Keywords: *DNA interaction, Dopamine, Iron oxide nanoparticles, Spectroscopy*

How to cite this article

Mehdipour M, Dehghan Gh R, Hosseinpour Feizi MA, Tarasi R, Khoobi M, Dastmalchi S. Spectroscopic investigation on the interaction of DNA with superparamagnetic iron oxide nanoparticles doped with chromene via dopamine as cross linker. Nanomed J. 2018; 5(1): 36-45. DOI: 10.22038/nmj.2018.05.006

INTRODUCTION

DNA plays an important role in biology and is the important target in cancer treatment, so the interaction of small molecules and DNA can damage the structure of DNA, blocks the proliferation of cancer cells and leads to cell death [1]. The interaction of small molecules with DNA has been extensively studied. These studies can get insights into the development of effective therapeutic drugs to control the gene expression [2]. The interaction between small molecules and DNA are of two types, covalent interactions and non-covalent interactions. The three major types of non-covalent interactions are; (a) electrostatic interactions that occurs between the negatively charged phosphate backbone of DNA and positively charged end of small molecules, (b) groove binding that involves hydrogen bonding or (c) Vander Waals interaction of the small molecules with nucleic acid bases and intercalative binding occurs when the small molecules intercalate

* *Corresponding Author Email: dehghan2001d@yahoo.com*

Note. This manuscript was submitted on October 5, 2017; approved on November 15, 2017

within the nucleic acid base pairs [3, 4].

In the recent development of biotechnology, magnetic nanoparticles have gained increasing attention for use in biomedical applications [5]. The multifunctional capabilities of engineered superparamagnetic iron oxide nanoparticles (SPIONPs) have profound impact on various fields of cancer therapeutics. They have potential to improve contrast features in magnetic resonance imaging (MRI) [6], drug delivery [7] and hyperthermia [8]. Because of their smaller size and hence greater surface to volume ratio and flexible surface modification properties, they have improved binding kinetics to the variety of substances. As SPIONPs are biodegradable and biocompatible, they find application in various biomedical fields such as gene therapy [9], cell and biological material separation [10]. SPIONPs need to have surface modification to improve their efficacy in clinical applications. Solubility, biocompatibility and stability are three main factors endowed with surface functionalization [11]. A widely used robust and versatile anchor on the surface of iron oxide nanoparticles is dopamine [12-14]. The linkage is based on the chelation of the hydroxyl groups of dopamine with the surface iron atoms rendering the particles at the same time water dispersible. The amine-functions on dopamine are one of the best parts for post-functionalization of the dopamine coated magnetic nanoparticles [15]. Pyranochromenes are one of the most commonly encountered oxygen containing heterocycles [16], which form the important compounds having medical significance [17-19].

Although a wide variety of methods are being used in cancer therapy, the magnetic nanoparticles seem to hold the greatest potential of success. By using nanoimaging and nanodrug delivery systems, cancer cells can be selectively targeted thus, reduce undesired systemic drug toxicity. In the present study we have tried to survey interaction of superparamagnetic iron oxide nanoparticles (SPIONs) doped with 2H-chromene via dopamine as cross linker (SPIONs@DA-Chr, Fig 1) with ctDNA and introduce SPIONs@DA-Chr as a new nanoparticle that target the DNA. The interaction properties of SPIONs@DA-Chr with calf thymus DNA were studied by using the UV-Vis spectrophotometry, fluorescence spectroscopy, CD and FT-IR spectroscopy, and viscosity measurement. This work will contribute to elucidating the binding mechanism of SPIONs@DA-Chr with DNA and will provide valuable information about behavior and mutual interactions of superparamagnetic nanoparticles with biological systems.

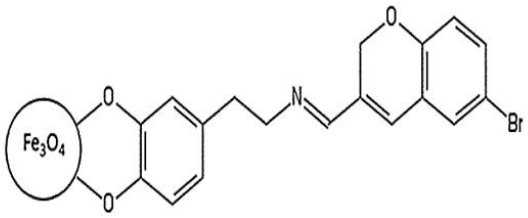

Fig 1. Structure of SPIONs@DA-Chr

MATERIALS AND METHODS

Materials

Calf thymus DNA (ctDNA) was purchased from sigma chemical company and used without further purification. Its stock solution was prepared by dissolving an appropriate amount of ctDNA in 10 mM Tris-HCl buffer (pH 7.4) and stored at 4°C. The concentration of DNA was determined by UV absorption spectroscopy using the molar absorption coefficient ε = 6600 M^{-1} cm^{-1} at 260 nm [20]. A solution of ctDNA gave a ratio of UV absorbance at 260 and 280 nm more than 1.8, which indicates that DNA was adequately free from protein [21].

Apparatus and methods

Synthesis and characterization of SPIONs@DA-Chr

SPIONs were synthesized by the chemical co-precipitation method [22]. For surface modification of SPIONs briefly, in first step 2 gr of dried SPIONs were well dispersed in 15 ml deionized water by using ultrasonic waves. After that, 4 gr of dopamine were dispersed in 15 ml deionized water and added to SPIONs under nitrogen atmosphere, NaOH (0.01 M) was dripped to the reaction mixture (pH 8), and the solution was stirred for 24h at RT. The resulting black precipitation was then collected by external magnet and washed three times by deionized water and acetone respectively. The obtained SPIONs@DA was dried under vacuum at 60°C overnight. In second step 500 mg of SPIONs@DA were dispersed in 200 ml ethanol and 500 mg of 6-bormo-2H-chromene-3-carbaldehyde was added to the SPIONs@DA solution, and the reaction mixture was stirred for 24h under the nitrogen atmosphere. Finally, precipitation collected by external magnet and

washed by acetone and ethanol. The obtained SPIONs@DA-Chr was dried under vacuum at 60°C overnight. SPIONs@DA-Chr were suspended in 10 mM Tris-HCl buffer containing 0.7% DMSO and sonicated to ensure a uniform suspension.

The SPIONs@DA-Chr was characterized by using Bruker Tensor 27 (Japan) FT-IR spectrometer, PG Instrument (T60, PG Instruments Ltd, Leicestershire, UK) UV-Vis spectrophotometer and LEO 1430VP (England & German) scanning electron microscopy (SEM).

Spectroscopic studies

The interaction between ctDNA and SPIONs@DA-Chr was studied by UV-Vis spectroscopy using PG Instrument (T60, PG Instruments Ltd, Leicestershire, UK) spectrophotometer. All experiments were accomplished in Tris-HCl buffer (10mM pH 7.4) by using a (1cm) quartz cell. Spectral changes of DNA were recorded after adding different concentrations of SPIONs@DA-Ch. Absorption spectrum has also been monitored under the same condition after adding different concentrations of ctDNA keeping constant SPIONs@DA-Chr concentration.

Fluorescence measurements were carried out in a JASCO (FP-750) (Japan) spectrofluorometer by using a quartz cell of 1cm path length. Excitation and emission slit were set at 5 nm. The fluorescence quenching measurements were determined by keeping the concentration of SPIONs@DA-Chr constant (15 µM) and varying the concentration of ctDNA (0-105 µM). Solutions were excited at 290 nm and the emission was monitored at 535 nm. For thermal study, samples were incubated at three different temperatures (298, 310 and 318 K) and some quantitative analysis were performed [23].

For competitive fluorescence assay, at first DNA (50µM) was added to methylene blue (MB) (50µM) solution and titrated with varied concentration of SPIONs@DA-Chr (0-6 µM). Samples were excited at 630 nm, and emission spectra were recorded from 650-730 nm.

CD spectra were recorded in a JASCO (J-810) (Japan) spectropolarimeter by adding various concentrations of SPIONs@DA-Chr (0-5.25 µM) and constant concentration of DNA (50 µM).

FT-IR spectra were obtained using a Bruker Tensor 27 (Japan) spectrometer at room temperature in a range of 4000-400 cm^{-1}. The samples were placed in a potassium bromide (KBr) disks.

Viscosity measurement was carried out in a viscometer (Ubbelohde-Iran) which was maintained at a constant temperature at 25 ± 0.1°C in a thermostatic water-bath. The ctDNA was fixed at 50 µM and SPIONs@DA-Chr was 0-5 µM. Flow time was measured with a digital stopwatch, the mean value of three replicated measurements was used to evaluate the viscosity (η) of the samples. The data were reported as $(\eta/\eta_0)^{1/3}$ versus the [compound/DNA] ratio. Where, η_0 is the viscosity of DNA solution alone [21].

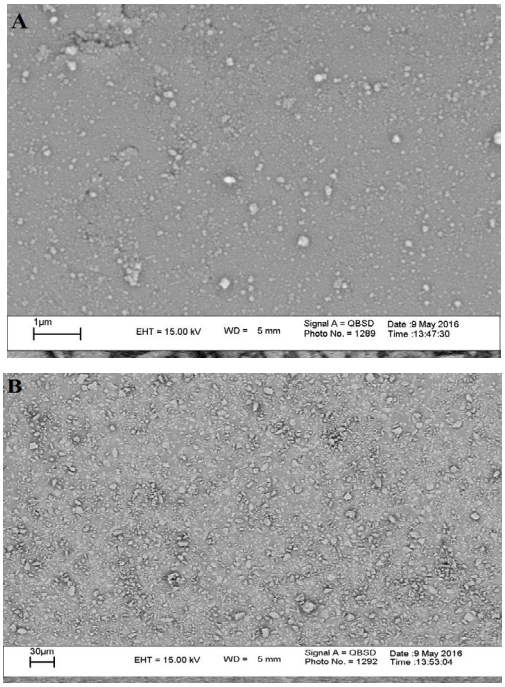

Fig 2. SEM image of Fe3O4 NPs (A: bare Fe3O4 NPs, B: SPIONs@DA-Chr)

RESULTS AND DISCUSSION

Characterization of SPIONs@DA-Chr

SEM images of bare Fe_3O_4 NPs and SPIONs@DA-Chr are shown in Fig 2. Fig 2a, shows that Fe_3O_4 NPs have uniform spherical shaped morphology. SPIONs@DA-Chr has different morphology than the naked Fe_3O_4 NPs, (Fig 2b). Slight increase in the size could be related to the surface modification. SPIONs@DA-Chr had 20-40 nm size. The absorption spectra of bare Fe_3O_4 and SPIONs@DA-Chr are shown in Fig 3. There are new peaks at 290 and 374 nm in the absorption spectra of SPIONs@DA-Chr that related to dopamine and chromene.

To certificate the successfully bonded of dopamine and chromene to Fe_3O_4 NPs, FT-IR analysis carried out. Fe_3O_4 NPs showed an absorption peak around 571 cm^{-1} assigned to the

Fe-O stretching of the iron oxide nanoparticles (Fig 4a). The broad band at 3423 cm^{-1} ascribed to the vibration of the hydroxyl groups and/or absorbed water molecules on the surface of the particles [24]. The spectrum of SPIONs@DA-Chr exhibit additional bands, (Fig 4b).The absorption bands appeared at 1644 and 1477 cm^{-1}could be related to the asymmetric and symmetric stretching vibration of the benzene rings. The bands related to the C-O bonds was located at 1284 cm^{-1}[25]. Also the peak at 631 cm^{-1} could be corresponded to the C-Br strong stretching [26]. All the above can demonstrate successfully formation of the SPIONs@DA-Chr.

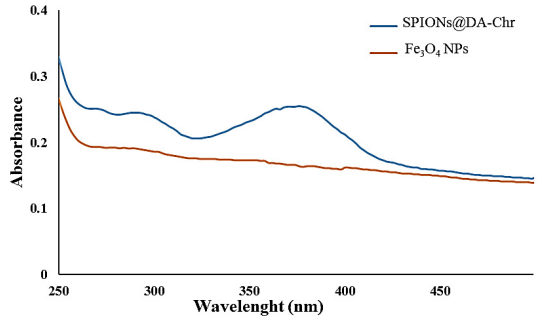

Fig 3. Absorption spectra of Fe3O4 NPs and SPIONs@DA-Chr

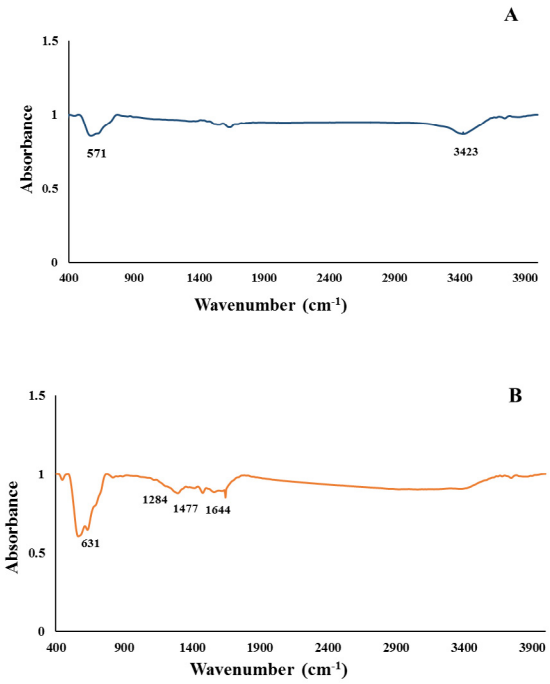

Fig 4. The FT-IR spectra of A: Fe3O4 NPs, B: SPIONs@DA-Chr

UV-Vis spectral measurements

Absorption spectroscopy is an effective technique that is useful to determine the binding mode of DNA with small molecules [27, 28]. Therefore, to demonstrate the binding possibility of the SPIONs@DA-Chr to ctDNA, spectroscopic titration was performed. UV spectra of SPIONs@DA-Chr (10 µM) in the presence of different concentrations of DNA (0-51 µM) are shown in Fig 5a. The absorption bands at 374 nm showed an increase in the peak intensities (hyperchromism) and slight blue shift with respect to increasing concentration of ctDNA. This change in the spectrum of SPIONs@DA-Chr in the presence of ctDNA is related to a non-intercalative binding mode. Amine and hydroxyl groups could form hydrogen bonds with the DNA base pairs, contributing to the overall hyperchromism [29]. The band at 260 nm of DNA arises from the π→π* electronic transition of the bases [30]. The absorption spectra related to the interaction of ctDNA with SPIONs@DA-Chr was recorded at a constant DNA concentration (50µM) and different concentrations of SPIONs@DA-Chr (0-6 µM), (Fig 5b). Generally hypochromism arises from the DNA helix axis, as well as its conformational changes, in contrast, hyperchromism is due to a damage of the ctDNA double-helix structure [31]. The changes observed in the absorption spectra of ctDNA in the presence of SPIONs@DA-Chr indicated the damage in the DNA double-helical structure and binding mode is non-intercalative. The value of the apparent association constant, K obtained from Benesi-Hildebrand equation (1) [32]:

$$\frac{A_0}{A - A_0} = \frac{\varepsilon_G}{(\varepsilon_{H\text{-}G} - \varepsilon_G)} + \frac{\varepsilon_G}{(\varepsilon_{H\text{-}G} - \varepsilon_G)} \cdot \frac{1}{K[CT - DNA]} \qquad (1)$$

Where "K" is the apparent association constant, A_0 and A are the absorbance of the SPIONs@DA-Chr and its complex with DNA, respectively, and ε_G and $\varepsilon_{H\text{-}G}$ are absorption coefficients of the SPIONs@DA-Chr and SPIONs@DA-Chr-DNA complex, respectively [32]. The association constant for SPIONs@DA-Chr was calculated 1.58×10^3 M^{-1}. This value of K was lower than that of classical intercalators, by comparing the calculated K with popular DNA binders [33], SPIONs@DA-Chr can interact with DNA through groove binding mode.

Fluorescence quenching studies

To study the interaction of small molecules with biomacromolecules, fluorescence spectroscopy is

the most suitable technique [34]. To investigate the binding mode of SPIONs@DA-Chr to ctDNA, the fluorescence titration experiment was performed. The emission spectrum of SPIONs@DA-Chr in the absence or presence of ctDNA was shown in Fig 6.

It was obvious that SPIONs@DA-Chr had a significant maximum emission peak at 535 nm following excitation at 290 nm. By increasing the concentration of ctDNA, the fluorescence intensity of the SPIONs@DA-Chr was decreased without any remarkable shift in the maximum wavelength of emission. Fluorescence quenching of SPIONs@DA-Chr can be described by Stern-Volmer equation (2) [35]:

$$\frac{F_0}{F} = 1 + K_q \tau_0 [Q] = 1 + K_{SV}[Q] \qquad (2)$$

Where F_0 and F represent the fluorescence intensities before and after the addition of the quencher (DNA), respectively. K_q is the fluorophore quenching rate constant, K_{SV} is Stern-Volmer constant, τ_0 is the life time of the fluorophore, and [Q] is the concentration of quencher [36]. From the slope of the plot in Fig 7, the Stern-Volmer quenching constant was calculated. The fluorescence quenching mechanisms are usually classified as dynamic and/or static quenching [37].

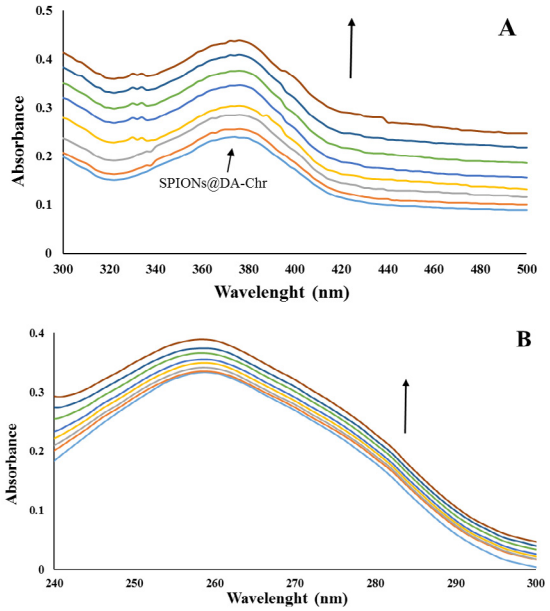

Fig 5. (A) Changes of UV spectra of SPIONs@DA-Chr (10 µM) in the presence of different concentrations of ctDNA (0-51µM). (B) Absorption spectra of ctDNA (50µM) in the presence of different concentrations of SPIONs@DA-Chr (0-6 µM)

Table 1. The Stern-Volmer constants, quenching constants of SPIONs@DA-Chr-DNA complex at different temperatures

T	R	K_{SV} (L/mol) 10^{-2}	K_q (L/mol/S) 10^{10}
298	0.9685	2.5	2.5
310	0.9853	2.8	2.8
318	0.9609	3.5	3.5

Dynamic quenching refers to a process that the fluorophore and the quencher come into contact during the transient existence of the excited state. This type of quenching depends upon diffusion. As regards higher temperature lead to larger diffusion coefficients, by rising the temperature K_{SV} can be increased. In the case of static quenching, fluorophore-quencher complex accomplishes. Complex stability can be decreased by increasing temperature, and therefore lower values of K_{SV} were resulted [38, 39]. The calculated K_{SV} at different temperatures (298, 310 and 318 K) is presented in Table 1. The results show that K_{SV} values were increased with increase in temperature indicating the dynamic type of quenching mechanism through interaction between DNA and SPIONs@DA-Chr.

Equilibrium binding titration

Fluorescence titration data were used to determine the binding constant (K_f) and the number of binding sites (n) by the following Eq (3) [40].

$$\log \frac{F_0 - F}{F} = \log K_f + n \log [Q] \qquad (3)$$

Where F_0 and F are the fluorescence intensities of the fluorophore in the absence and presence of different concentrations of quencher, respectively. A plot of log [(F_0 – F/F)] vs. log [Q] yields a slope equal to n and the length of intercept on Y-axis equals to logK_f (Fig 8).

The values of K_f and n are shown in Table 2. The low binding constant (K_f) of SPIONs@DA-Chr in comparison with intercalators [41, 42], demonstrated that SPIONs@DA-Chr binds to ctDNA via groove binding mode.

Table 2. Binding constants (Kf) and number of binding sites (n) of SPIONs@DA-Chr-DNA complex at different temperatures

T	R	K_f (L/mol) 10^4	n
298	0.9596	0.1	1.5
310	0.9281	2.5	1.2
318	0.9045	19.9	0.9

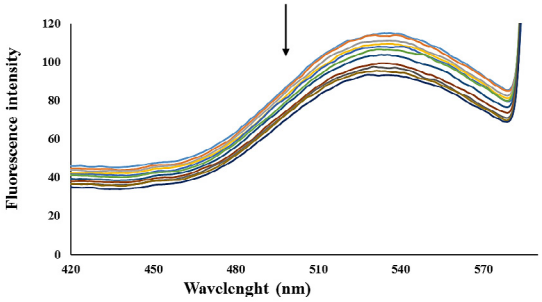

Fig 6. Fluorescence spectra of the SPIONs@DA-Chr in the absence and presence of increasing concentrations of ctDNA (0-105 µM) at 298 K

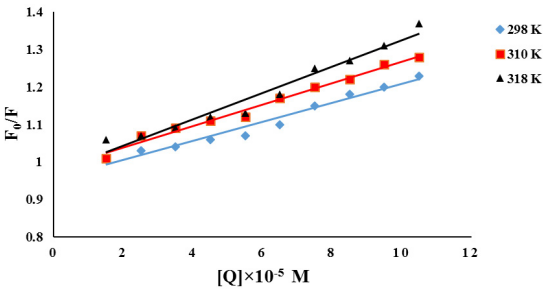

Fig 7. Stern-Volmer plot of ctDNA- SPIONs@DA-Chr complex at different temperatures (298, 310 and 318 K)

Thermodynamic studies

The interaction forces between small molecules and biomolecules mainly contain hydrogen bonds, Van der Waals forces, electrostatic forces and hydrophobic interactions [43]. If ΔH > 0, ΔS > 0, the main acting force is hydrophobic interaction; if ΔH < 0, ΔS > 0, the major force is the electrostatic effect; if ΔH < 0, ΔS < 0, the main binding force is Van der Waals force or hydrogen bond [44]. To determine the interaction force of SPIONs@DA-Chr with ctDNA, we calculated the thermodynamic parameters from the Van't Hoff equation (4):

$$\ln K_f = -\frac{\Delta H}{RT} + \frac{\Delta S}{R} \quad (4)$$

$$\Delta G = \Delta H - T\Delta S \quad (5)$$

ΔH and ΔS were determined by the plotting $\ln K_f$ versus 1/T (Fig 9). The free energy change (ΔG) was estimated from Eq (5). The values of ΔH, ΔS and ΔG for the interaction of SPIONs@DA-Chr and ctDNA are shown in Table 3. Negative value of ΔG is responding to spontaneous interaction process and positive ΔH and ΔS indicated that the hydrophobic force was a major binding force between SPIONs@DA-Chr and DNA.

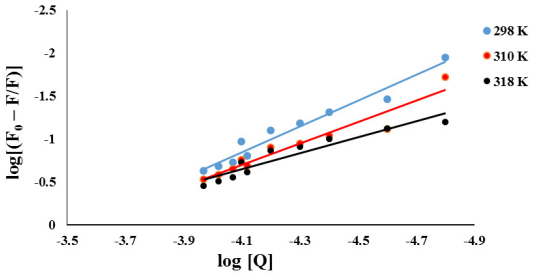

Fig 8. Determination of binding constant and number of binding site from double logarithm plot of fluorescence quenching

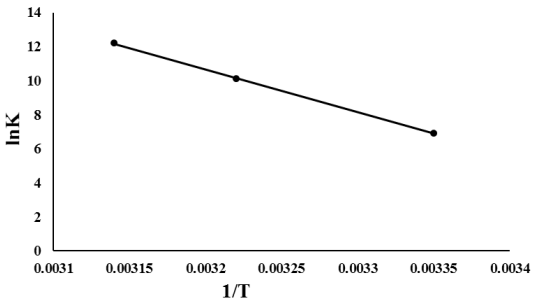

Fig 9. Van'n Hoff plot of SPIONs@DA-Chr-DNA complex

Competitive study using methylene blue (MB)

The competitive study was carried out using methylene blue (MB). MB can bound to duplex DNA via intercalation. The emission intensity of MB was quenched on adding DNA due to its strong stacking interaction (intercalation) between the DNA base pairs. The fluorescence of MB decreased after binding with DNA due to its intercalation [33, 45]. If MB was replaced with SPIONs@DA-Chr, it could lead to a significant increase in the fluorescence intensity of MB-DNA complex. Fig 10 shows the fluorescence emission spectra of MB with and without ctDNA and the effect of adding increasing concentration of SPIONs@DA-Chr to MB-DNA. There is not clearly change in the fluorescence intensity of MB upon addition of SPIONs@DA-Chr. Although, the binding constant of SPIONs@DA-Chr is higher than MB (2.13×10^4 M^{-1}), but it is not able to release MB, because they have different binding sites. This result is an evidence for a non-intercalative mode of binding.

Circular dichroism spectroscopy

CD is an useful technique in diagnosing structural changes in DNA during ligand-DNA interactions, as the positive band due to base stacking (275 nm) and the negative one due to

right handed helicity (245 nm) are quite sensitive to the mode of DNA interactions with small molecules [46]. The shift in the CD signals of DNA due to interaction of ctDNA with compounds may often be designated to the corresponding changes in the DNA structure [47]. Classical intercalative molecules usually tend to enhance the intensities of bands due to strong base stacking interactions and stable DNA conformations, while simple groove binding and electrostatic interactions demonstrate less or no perturbation on the base stacking and helicity bands [48].

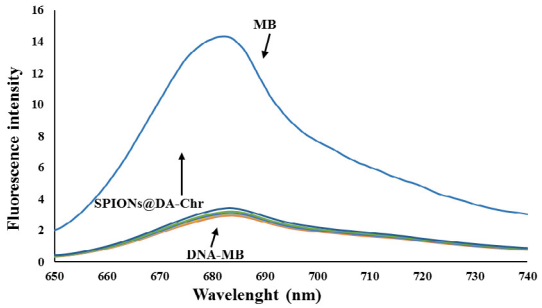

Fig 10. Emission spectra of MB-DNA in the presence of increasing amount of SPIONs@DA-Chr (0-6 µM)

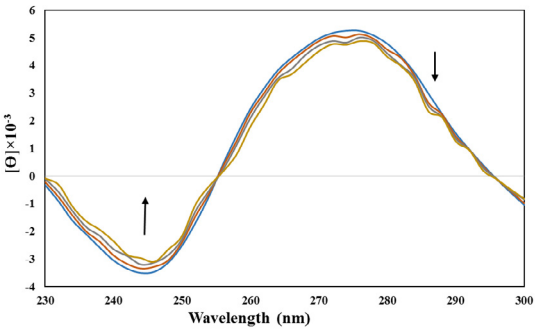

Fig 11. CD spectra of ctDNA (50µM) in 10 mM Tris-HCl buffer, in the presence of increasing concentrations of SPIONs@DA-Chr (0, 2.25, 4.25, 5.25 µM). The arrows show the CD spectra changes

The CD spectra of DNA in the presence of SPIONs@DA-Chr are illustrated in Fig 11. After adding different concentrations of SPIONs@DA-Chr, the intensities of positive and negative bands were decreased. According to CD spectra it can be assumed that SPIONs@DA-Chr may not significantly change the helicity of DNA. Also it is important evidence for the groove binding of SPIONs@DA-Chr to ctDNA that confirms our other findings. This result is similar to the results of silver nanoparticles interaction with ctDNA [49].

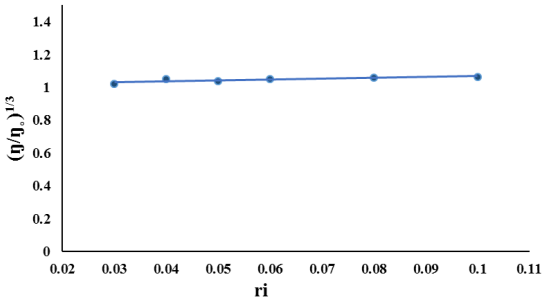

Fig 12. Effect of increasing amount of SPIONs@DA-Chr (0-5 µM) on the viscosity of ctDNA (50 µM)

Table 3. Thermodynamic parameters for SPIONs@DA-Chr-DNA binding at different temperatures

T	R	ΔH (KJ/mol)	ΔS (J/mol/K)	ΔG (KJ/mol)
298	0.9997	25.17	91.226	-2.01
310	0.9997	25.17	91.226	-3.11
318	0.9997	25.17	91.226	-3.8

Viscosity measurement

To confirm the binding mode of SPIONs@DA-Chr with DNA viscosity measurement carried out. Hydrodynamic methods, such as determination of viscosity, can be considered to be highly sensitive to the change in length of DNA. A classical intercalation model illustrates lengthening of DNA helix with the separation of DNA base pairs for adapting the bound molecule, leading to the increase in DNA viscosity. Overhand, a partial, non-classical intercalation of molecules could bend the DNA helix, reducing its length and subsequently, its viscosity. Furthermore molecules that binds exclusively in the DNA groove by partial and/or non-classical intercalation typically cause less (positive or negative) or no change in DNA solution viscosity [43]. The effect of different concentrations of SPIONs@DA-Chr (0-5 µM) on the viscosity of ctDNA is shown in Fig 12. Results show only a slight increase in the viscosity of DNA while increasing concentration of SPIONs@DA-Chr, which indicates that groove binding mode of interaction is more probable.

FT-IR spectra of SPIONs@DA-Chr-DNA complex

Fig 13 shows the FT-IR spectra of free DNA and DNA bound with SPIONs@DA-Chr. The vibrational frequencies of the NH and OH groups of free DNA appeared around 3414-3478 cm^{-1} [40], and in the SPIONs@DA-Chr-DNA complex had a little shift to 3415-3478 cm^{-1}. This broad band in free DNA is mainly attributed to the intramolecular H-bonding and the changing in NH band on NPs interaction

is indicative of the interaction of SPIONs@DA-Chr with DNA bases. The Guanine band at 1796 cm^{-1}, Adenine at 1617 cm^{-1}, Cytosine at 1510 cm^{-1} and the band at 1637 cm^{-1} related to Thymine [50], shifted slightly toward lower frequencies at 1772, 1617,1510 and 1636 cm^{-1}, respectively. Thereupon the NPs show affinity to DNA bases respectively G>T>A>C. The asymmetric phosphate anion (PO^-_2) stretching band at 1365 cm^{-1} in free DNA, has been omitted in complex and symmetric vibration at 1036 cm^{-1} shifted to 1182 cm^{-1}. Also the IR B-marker bands at 896 cm^{-1} for sugar-phosphate stretch and 865 cm^{-1} for phosphodiester mode present in free DNA [51, 52], changed in SPIONs@DA-Chr-DNA complex. These results indicated that the secondary structure of DNA was changed via interaction of SPIONs@DA-Chr with DNA.

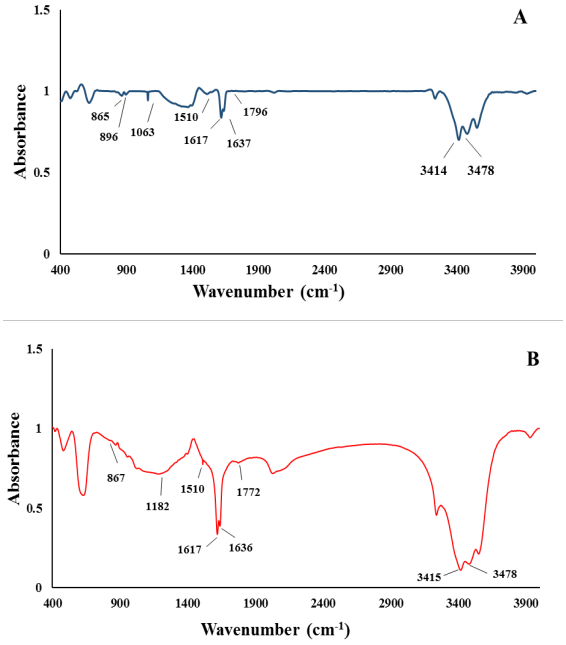

Fig 13. FT-IR spectra of (A) free DNA, (B) SPIONs@DA-Chr-DNA complex

CONCLUSION

DNA binding mechanism of SPIONs@DA-Chr was studied in the present research. SPIONs@DA-Chr was characterized by using SEM and FT-IR spectroscopic methods. The interaction of NPs with ctDNA was studied by various spectroscopic methods and viscosity measurement. All the results indicate that SPIONs@DA-Chr binds to DNA through groove binding mode. The quenching mechanism, binding constant and binding force were obtained from the fluorescence quenching. These results suggest the potential of SPIONs@DA-Chr to target the DNA and design the effective anticancer compounds.

ACKNOWLEDGMENTS

The authors are grateful to the University of Tabriz and Drug Applied Research center, Tabriz University of Medical Science, for their help in this research.

CONFLICT OF INTEREST

The authors declare no conflicts of interests.

REFERENCES

1. Yang L, Fu Z, Niu X, Zhang G, Cui F, Zhou C. Probing the interaction of anthraquinone with DNA by spectroscopy, molecular modeling and cancer cell imaging technique. Chem Biol Interact. 2015; 233: 65-70.
2. Srivastva AN, Singh NP, Shriwastaw CK. In vitro antibacterial and antifungal activities of binuclear transition metal complexes of ONNO Schiff base and 5-methyl-2,6-pyrimidine-dione and their spectroscopic validation. Arabian J Chem. 2016; 9(1): 48-61.
3. Hasanzadeh M, Shadjou N. Pharmacogenomic study using bio-and nanobioelectrochemistry: Drug–DNA interaction. Mater Sci Eng C Mater Biol Appl. 2016; 61: 1002-1017.
4. Shabbir M, Ahmad I, Ismail H, Ahmed S, McKee V, Akhter Z, Mirza B. Pharmacological, electrochemical and drug–DNA interaction aspects of tridentate Schiff bases and their triphenylphosphine nickel(II) complexes. Polyhedron. 2017; 133: 270-278.
5. Sood A, Arora V, Shah J, Kotnala R, Jain TK. Multifunctional gold coated iron oxide core-shell nanoparticles stabilized using thiolated sodium alginate for biomedical applications. Mater Sci Eng C Mater Biol Appl. 2017; 80: 274-281.
6. Wang Z, Qiao R, Tang N, Lu Z, Wang H, Zhang Z, Xue X, Huang Z, Zhang S, Zhang G. Active targeting theranostic iron oxide nanoparticles for MRI and magnetic resonance-guided focused ultrasound ablation of lung cancer. Biomaterials. 2017; 127: 25-35.
7. Dhal S, Mohanty A, Yadav I, Uvanesh K, Kulanthaivel S, Banerjee I, Pal K, Giri S. Magnetic nanoparticle incorporated oleogel as iontophoretic drug delivery system. Colloids Surf B Biointerfaces. 2017; 157: 118-129.
8. Soares PI, Laia CA, Carvalho A, Pereira LC, Coutinho JT, Ferreira IM, Novo CM, Borges JP. Iron oxide nanoparticles stabilized with a bilayer of oleic acid for magnetic hyperthermia and MRI applications. Appl Surf Sci. 2016; 383: 240-247.
9. Shalaby SM, Khater MK, Perucho AM, Mohamed SA, Helwa I, Laknaur A, Lebedyeva I, Liu Y, Diamond MP, Al-Hendy AA. Magnetic nanoparticles as a new approach to improve the efficacy of gene therapy against differentiated human uterine fibroid cells and tumor-initiating stem cells. Fertil Steril. 2016; 105(6): 1638-1648.
10. Kwak B, Lee J, Lee D, Lee K, Kwon O, Kang S, Kim Y. Selective isolation of magnetic nanoparticle-mediated heterogeneity subpopulation of circulating tumor cells using magnetic gradient based microfluidic system. Biosens Bioelectron. 2017; 88: 153-158.
11. Kang T, Li F, Baik S, Shao W, Ling D, Hyeon T. Surface design

of magnetic nanoparticles for stimuli-responsive cancer imaging and therapy. Biomaterials. 2017; 136: 98-114.
12. Lin L-S, Cong Z-X, Cao J-B, Ke K-M, Peng Q-L, Gao J, Yang H-H, Liu G, Chen X. Multifunctional Fe3O4@ polydopamine core–shell nanocomposites for intracellular mRNA detection and imaging-guided photothermal therapy. ACS Nano. 2014; 8(4): 3876-3883.
13. Sherwood J, Xu Y, Lovas K, Qin Y, Bao Y. Surface functionalization of dopamine coated iron oxide nanoparticles for various surface functionalities. J Magn Magn Mater. 2017; 427: 220-224.
14. Wan X, Zhan Y, Long Z, Zeng G, Ren Y, He Y. High-performance magnetic poly (arylene ether nitrile) nanocomposites: Co-modification of Fe3O4 via mussel inspired poly (dopamine) and amino functionalized silane KH550. Appl Surf Sci. 2017; 425: 905-914.
15. Gu X, Zhang Y, Sun H, Song X, Fu C, Dong P. Mussel-inspired polydopamine coated iron oxide nanoparticles for biomedical application. J Nanomater. 2015; 2015: 1-12.
16. Lasemi Z, Azimi R, Azizi Amiri M. Efficient synthesis of 9, 10-dihydropyrano [2, 3-h] chromene-2, 8-dione derivatives in ionic liquid and the study of their antioxidant activity. Nat Prod Res. 2017; 31(1): 1-6.
17. Ruan B-F, Cheng H-J, Ren J, Li H-L, Guo L-L, Zhang X-X, Liao C. Novel 2H-chromen-2-one derivatives of resveratrol: design, synthesis, modeling and use as human monoamine oxidase inhibitors. Eur J Med Chem. 2015; 103: 185-190.
18. Mokale SN, Begum A, Sakle NS, Shelke VR, Bhavale SA. Design, synthesis and anticancer screening of 3-(3-(substituted phenyl) acryloyl)-2H-chromen-2ones as selective anti-breast cancer agent. Biomed Pharmacother. 2017; 89: 966-972.
19. de Oliveira SGD, Lund RG, de Carvalho RV, de Pereira CMP, Piva E. Anti-candida and anti-enzyme activity and cytotoxicity of 2-phenyl-4H-chromen-4-one. Afr J Microbiol Res. 2016; 10(7): 219-224.
20. Nithya P, Helena S, Simpson J, Ilanchelian M, Muthusankar A, Govindarajan S. New cobalt(II) and nickel(II) complexes of benzyl carbazate Schiff bases: Syntheses, crystal structures, in vitro DNA and HSA binding studies. J Photochem Photobiol B. 2016; 165: 220-231.
21. Zhao T, Bi S, Wang Y, Wang T, Pang B, Gu T. In vitro studies on the behavior of salmeterol xinafoate and its interaction with calf thymus DNA by multi-spectroscopic techniques. Spectrochim Acta A Mol Biomol Spectrosc. 2014; 132: 198-204.
22. Motevalizadeh SF, Khoobi M, Sadighi A, Khalilvand-Sedagheh M, Pazhouhandeh M, Ramazani A, Faramarzi MA, Shafiee A. Lipase immobilization onto polyethylenimine coated magnetic nanoparticles assisted by divalent metal chelated ions. J Mol Catal B Enzym. 2015; 120: 75-83.
23. Hassan MF, Rauf A. Synthesis and multi-spectroscopic DNA binding study of 1, 3, 4-oxadiazole and 1, 3, 4-thiadiazole derivatives of fatty acid. Spectrochim Acta A Mol Biomol Spectrosc. 2016; 153: 510-516.
24.Kaminska I, Das MR, Coffinier Y, Niedziolka-Jonsson J, Sobczak J, Woisel P, Lyskawa J, Opallo M, Boukherroub R, Szunerits S. Reduction and functionalization of graphene oxide sheets using biomimetic dopamine derivatives in one step. ACS Appl Mater Interfaces. 2012; 4(2): 1016-1020.
25. Adhikary J, Datta A, Dasgupta S, Chakraborty A, Menéndez MI, Chattopadhyay T. Development of an efficient magnetically separable nanocatalyst: theoretical approach on the role of the ligand backbone on epoxidation capability. RSC Adv. 2015; 5(112): 92634-92647.
26. Barroso-Bogeat An, Alexandre-Franco M, Fernández-González C, Gómez-Serrano V. FT-IR analysis of pyrone and chromene structures in activated carbon. Energy Fuels. 2014; 28(6): 4096-4103.
27. Dehkordi MF, Dehghan G, Mahdavi M, Feizi MAH. Multispectral studies of DNA binding, antioxidant and cytotoxic activities of a new pyranochromene derivative. Spectrochim Acta A Mol Biomol Spectrosc. 2015; 145: 353-359.
28. Roy S, Sadhukhan R, Ghosh U, Das TK. Interaction studies between biosynthesized silver nanoparticle with calf thymus DNA and cytotoxicity of silver nanoparticles. Spectrochim Acta A Mol Biomol Spectrosc. 2015; 141: 176-184.
29. Patel MN, Gandhi DS, Parmar PA, Mehta JV. Molecular docking, free radical scavenging, and DNA interaction studies of drug-based coordination compounds. Monatsh Chem. 2017; 148(5): 901-908.
30. Rahman Y, Afrin S, Husain MA, Sarwar T, Ali A, Shamsuzzaman, Tabish M. Unravelling the interaction of pirenzepine, a gastrointestinal disorder drug, with calf thymus DNA: An in vitro and molecular modelling study. Arch Biochem Biophys. 2017; 625-626: 1-12.
31. Dehghan G, Dolatabadi JEN, Jouyban A, Zeynali KA, Ahmadi SM, Kashanian S. Spectroscopic studies on the interaction of quercetin–terbium (III) complex with calf thymus DNA. DNA Cell Biol. 2011; 30(3): 195-201.
32. Benesi HA, Hildebrand J. A spectrophotometric investigation of the interaction of iodine with aromatic hydrocarbons. J Am Chem Soc. 1949; 71(8): 2703-2707.
33. Vardevanyan PO, Antonyan AP, Parsadanyan MA, Torosyan MA, Karapetian AT. Joint interaction of ethidium bromide and methylene blue with DNA. The effect of ionic strength on binding thermodynamic parameters. J Biomol Struct Dyn. 2016; 34(7): 1377-1382.
34. Xiong X-L, You C, Xue K, Huang J-H, Wang C-L. Synthesis, characterization, and DNA binding studies of the hematoxylin-Zn(II) complex. Inorg Nano-Met Chem. 2017; 47(5): 794-799.
35. Arshad N, Zafran M, Ashraf Z, Perveen F. Synthesis, characterization of amide substituted dexibuprofen derivatives and their spectral, voltammetric and docking investigations for DNA binding interactions. J Photochem Photobiol B. 2017; 169: 134-147.
36. Mukherjee A, Singh B. Binding interaction of pharmaceutical drug captopril with calf thymus DNA: a multispectroscopic and molecular docking study. J Lumin. 2017; 190: 319-327.
37. Qais FA, Ahmad I. In vitro interaction of cefotaxime with calf thymus DNA: Insights from spectroscopic, calorimetric and molecular modelling studies. J Pharm Biomed Anal. 2018; 149: 193-205.
38. Murtaza S, Shamim S, Kousar N, Tahir MN, Sirajuddin M, Rana UA. Synthesis, biological investigation, calf thymus DNA binding and docking studies of the sulfonyl hydrazides and their derivatives. J Mol Struct. 2016; 1107: 99-108.
39. Yang C-Z, Liang C-Y, Zhang D, Hu Y-J. Deciphering the interaction of methotrexate with DNA: spectroscopic and molecular docking study. J Mol Liq. 2017; 248: 1-6.
40. Silva MM, Nascimento EO, Silva EF, de Araújo JX, Santana CC, Grillo LAM, de Oliveira RS, Costa PR, Buarque CD, Santos JCC. Interaction between bioactive compound

11a-N-tosyl-5-deoxi-pterocarpan (LQB-223) and Calf thymus DNA: Spectroscopic approach, electrophoresis and theoretical studies. Int J Biol Macromol. 2017; 96: 223-233.
41. Kocak A, Yilmaz H, Faiz O, Andac O. Experimental and theoretical studies on Cu(II) complex of N,N′ -disalicylidene-2,3-diaminopyridine ligand reveal indirect evidence for DNA intercalation. Polyhedron. 2016; 104: 106-115.
42. Tarushi A, Kakoulidou C, Raptopoulou CP, Psycharis V, Kessissoglou DP, Zoi I, Papadopoulos AN, Psomas G. Zinc complexes of diflunisal: Synthesis, characterization, structure, antioxidant activity, and in vitro and in silico study of the interaction with DNA and albumins. J Inorg Biochem. 2017; 170: 85-97.
43. Qais FA, Abdullah K, Alam MM, Naseem I, Ahmad I. Interaction of capsaicin with calf thymus DNA: A multi-spectroscopic and molecular modelling study. Int J Biol Macromol. 2017; 97: 392-402.
44. Sadeghi M, Bayat M, Cheraghi S, Yari K, Heydari R, Dehdashtian S, Shamsipur M. Binding studies of the anti-retroviral drug, efavirenz to calf thymus DNA using spectroscopic and voltammetric techniques. J Lumin. 2016; 31(1): 108-117.
45. Hegde AH, Seetharamappa J. Fluorescence and circular dichroism studies on binding and conformational aspects of an anti-leukemic drug with DNA. Mol Biol Rep. 2014; 41(1): 67-71.
46. Niroomand S, Khorasani-Motlagh M, Noroozifar M, Jahani S, Moodi A. Photochemical and DFT studies on DNA-binding ability and antibacterial activity of lanthanum (III)-phenanthroline complex. J Mol Struct. 2017; 1130: 940-950.
47. Roy S, Ganai S, Nandi R, Majundar K, Das T. Report of Interaction Between Calf Thymus DNA and Pyrimidine-Annulated Spiro-Dihydrofuran. Biochem Anal Biochem. 2016; 5(278): 2161-1009.
48. Moghadam NH, Salehzadeh S, Shahabadi N. Spectroscopic and molecular docking studies on the interaction of antiviral drug nevirapine with calf thymus DNA. Nucleosides Nucleotides Nucleic Acids. 2017; 36(9): 553-570.
49. Pramanik S, Chatterjee S, Saha A, Devi PS, Suresh Kumar G. Unraveling the Interaction of Silver Nanoparticles with Mammalian and Bacterial DNA. J Phys Chem B. 2016; 120(24): 5313-5324.
50. Saito S, Silva G, Santos RX, Gosmann G, Pungartnik C, Brendel M. Astragalin from Cassia alata induces DNA adducts in Vitro and repairable DNA damage in the yeast Saccharomyces cerevisiae. Int J Mol Sci. 2012; 13(3): 2846-2862.
51. Hemachandran H, Anantharaman A, Priya RR, Doss GP, Siva R. Interaction of Catechu Dye with DNA: Spectroscopic and In Silico Approach. Nucleosides Nucleotides Nucleic Acids. 2016; 35(4): 195-210.
52. Saeidifar M, Sohrabi Jam Z, Shahraki S, Khanlarkhani A, Javaheri M, Divsalar A, Mansouri-Torshizi H, Akbar Saboury A. Multi-spectroscopic and electrochemical approaches of the interaction between a new binuclear agent and DNA. J Biomol Struct Dyn. 2017; 35(12): 2557-2564.